PAPER

Check for updates

Qualitative and quantitative adsorption mechanisms of zinc ions from aqueous solutions onto dead carp derived biochar†

Hong-tao Qiao, [ID] [a] Yong-sheng Qiao, [a] Xiao-hang Luo, [a] Bao-wei Zhao [ID] *[b] and Qiu-ying Cai [a]

The objective of this study is to investigate the qualitative mechanisms of Zn^{2+} adsorption on carp biochars (CMBx) produced from dead carp at different temperatures (450–650 °C) and their quantitative contribution. The pseudo second order kinetic model and the Langmuir model could fit the kinetic and isothermal adsorption data well, respectively. The intra-particle diffusion was the main rate-limiting step but not the only rate-limiting step. The maximum adsorption capacity obtained from the Langmuir model for CMB650 was 87.7 mg g^{-1} which was greater than those of other biochars. Precipitation with minerals, ion exchange, and complexation with functional groups (OFGs) were the main adsorption mechanisms. Quantum chemistry calculations confirmed that the functional groups (*e.g.*, hydroxyl, carboxyl and C=C) tended to bind with Zn^{2+} more strongly than with Ca^{2+} and Mg^{2+}, because the structure of the complex formed by the former was more stable. The contribution of different adsorption mechanisms varied with the pyrolysis temperature to prepare biochar. With increasing pyrolysis temperature, the contribution of the interaction between Zn^{2+} and the minerals increased from 46.4% to 84.7%, while that of complexation with OFGs decreased from 41.7% to 4.7%. Overall, the mechanism of Zn^{2+} adsorption on CMB450 was dominated by complexation with OFGs and exchange with cations (accounting for 73.2%), while the mechanisms on CMB650 were dominated by the interaction with minerals. In view of the total adsorption capacity, 650 °C was the optimized pyrolysis temperature for CMBx preparation and adsorption treatment of Zn-contaminated water. These results are useful for screening effective biochars as engineered sorbents to treat Zn-containing wastewater.

1. Introduction

With the rapid development of industrialization and urbanization, massive amounts of zinc ion-containing wastewater (*e.g.*, industrial effluents, galvanized waste liquids, and leachates from landfills) are discharged into the environment. Although zinc ions are originally beneficial to the growth of human beings, animals and plants, they act as a heavy metal pollutant because of their excessive amounts.[1–4] Large amounts of Zn^{2+} could lead to strong toxicity for human beings and lead to serious environmental pollution and ecological damage (*e.g.*, Zn^{2+} with concentration > 5 mg L^{-1} in water).[5–7] In addition, compared to other heavy metal ions, Zn^{2+} ions are not readily removed from water environment due to their higher electronegativity.[7] Among the many treatment technologies for heavy

metal polluted water, the adsorption by biochar is considered to have broad application prospects.[8] Biochar is a kind of carbon-containing, stable and highly aromatized carbonaceous solid material prepared by pyrolysis of biomass (*e.g.*, plant residues, livestock and poultry manure, and other organic solid wastes) under oxygen-limited conditions and the temperature below 700 °C.[8–10] In recent years, China supplies about 60.5% of aquatic products worldwide.[11,12] The large amount of wastes (*e.g.*, dead or sick aquatic carcasses, residual baits and feces) that produced during the intensive farming process are burned or buried, which will cause not only waste of biomass energy and environmental pollution, but also risks of zoonotic diseases.[11,12] Alternatively, if these wastes were converted into biochar and employed for the removal of heavy metal ions (*e.g.* Zn^{2+}) from wastewater, it would be quite beneficial to resource utilization of waste and remediation of heavy metal polluted wastewater.

According to recently published research results, the mechanisms responsible for heavy metal adsorption on biochar mainly included physical adsorption, chemical precipitation, surface complexation with oxygen-containing functional groups (OFGs), cation exchange, electrostatic attraction, and cation–π

[a]Institute of Applied Chemistry, Department of Chemistry, Xinzhou Teachers University, Xinzhou 034000, China. E-mail: 469494248@qq.com

[b]School of Environmental and Municipal Engineering, Lanzhou Jiaotong University, Lanzhou 730070, China. E-mail: zhbw2001@sina.com

interaction.[13–18] However, the relative contribution of these mechanisms for heavy metal adsorption on biochar largely varies with the type of biomass and pyrolysis temperature. Specifically speaking, Zhao et al. indicated that for the biochars derived from rice straw, chicken manure, and sewage sludge at 350 and 550 °C, adsorption capacities and mechanisms for Pb^{2+} and Zn^{2+} were quite different.[18] Deng et al. found that for the rice straw biochars prepared at 400 and 700 °C, the contribution of complexation with surface acid groups was negligible and the dominant adsorption mechanisms for heavy metals on the low temperature biochar and high temperature biochar were cation exchange and precipitation with minerals respectively.[15] Additionally, Lei et al. reported that animal derived biochars (ADBs) were more effective in immobilizing Pb^{2+}, Cd^{2+} and Cu^{2+} than plant or manure derived biochars; and Pb^{2+} was effectively immobilized *via* precipitation, whereas ion exchange was the dominant mechanism in combining Cd^{2+} and Cu^{2+} with ADBs.[16,17] The reason is that the ADBs had large amount of hydroxyapatite (HAP) and relatively low carbon contents, and HAP had a significant effect on the adsorption of heavy metal ions on ADBs.[16,17,19,20] These results suggest that the quantitative information of different adsorption mechanisms is of great significance for the application of biochar in the remediation of heavy metal pollution. However, the qualitative and quantitative adsorption mechanism of Zn removal by aquatic animal biochar is still unknown, which makes it lack the necessary theoretical support for its application in the remediation of heavy metal pollution.

In order to fill this gap, dead carp was selected as the research object of aquatic animals, and the objectives of this work are to: (i) investigate the adsorption performance of Zn^{2+} on biochars prepared from dead carp at different pyrolysis temperature; (ii) understand the contributions of each mechanism to total adsorption by the biochars on a qualitative and quantitative basis; (iii) assess the removal potential of Zn^{2+} by biochars and discuss the relationship between the mechanisms and the specific properties of biochars. These results will have guiding significance for screening effective biochar as engineering adsorbent to treat Zn-containing wastewater.

2. Experimental

2.1 Biochar preparation and characterization

Dead carps were obtained from a fish farm in Xinzhou, Shanxi Province, China. Carp was cut into pieces, washed with distilled water, air-dried for 2 D, dried in an oven at 70 °C for 24 h to make carp meat and bone meal, and then crushed and passed through a 0.84 mm sieve (20 mesh). Carp biomass was tightly placed in a ceramic pot, and then pyrolyzed in the muffle furnace under limited air with a heating rate of 15 °C min^{-1} and held at the peak temperature (450, 550, and 650 °C) for 6 h before cooling to room temperature. All biochar samples were passed through a 0.17 mm sieve (80 mesh), and stored in airtight containers and labelled as CMB450, CMB550, and CMBC650 in accordance with the pyrolysis temperature, respectively. Demineralized biochars were obtained according

to the method by Wang et al.[21] and identified as DCMB450, DCMB550, and DCMB650, respectively (ESI†).

The physicochemical (yield, zeta potential, pH, specific surface area, elemental composition and thermogravimetric curves) and spectral (SEM-EDS, XRD, XPS and FTIR) properties of biochars were measured. More detailed analytical methods were described in the ESI.†

2.2 Adsorption experiments

Batch adsorption experiments were carried out to elucidate the characteristics of Zn^{2+} adsorption on biochars. A certain amount of biochars (0.02 g) was added into a 50 mL conical flask, and mixed with 20 mL solutions containing initial Zn^{2+} concentration. The initial pH value for Zn^{2+} solutions was adjusted to 5.0 ± 0.05 by adding 0.1 M HNO_3 or NaOH solutions and the tested Zn^{2+} solutions for the adsorption experiments contained 0.01 M $NaNO_3$ (analytical reagent, Sinopharm, China) as background electrolyte to keep a constant ionic strength. The mixture was shaken in the air bath thermostat oscillator (THZ-82A, Putian Instrument Manufacturing Co., Ltd., China) at 150 rpm and 25 °C for a certain time. The mixture was filtered with a 0.45 μm filter membrane after shaking, and the filtrate was used to measure of Zn^{2+} concentration by inductively coupled plasma emission spectrometer (ICP-OES) (Optima 8000, PerkinElmer, USA). For adsorption kinetics experiments, the initial Zn^{2+} concentration was 100 mg L^{-1} and the oscillating adsorption time was 2–420 min. Adsorption isotherm experiments were carried out as mentioned above with initial Zn^{2+} concentrations in the range of 60–500 mg L^{-1} for 7 h. Kinetic and isothermal adsorption models were used to illustrate the adsorption process, and the fitting analysis was described in the ESI.†

In order to illustrate the contribution of each mechanism to the overall adsorption of Zn^{2+} on biochars, the CMBx ('x' represents the pyrolysis temperature of biochar) and DCMBx were placed into Zn^{2+} solution (100 mg L^{-1}), and distilled water as a contrast under the same conditions above, respectively. Then, the pH values and the concentrations of K^+, Ca^{2+}, Na^+, Mg^{2+} and Zn^{2+} in solutions were measured and analyzed by the pH meter and ICP-OES after filtering through 0.45 μm filters. The biochars loaded with Zn^{2+} were individually collected for FTIR, XRD, XPS and SEM-EDS analyses.

2.3 Quantitative contributions of different mechanisms to Zn^{2+} adsorption on biochars

The contributions of Zn^{2+} adsorption mechanisms on CMBx were determined using the method reported by Cui et al.,[13] Wang et al.,[22] Deng et al.[15] and further modified by Gao et al.[8] The specific calculation methods about the contributions of precipitation with minerals (Q_{pm}), exchange with cation (Q_{ec}), complexation with OFGs (Q_{cf}) and other potential mechanisms (Q_{op}) (including physical adsorption and Zn^{2+}–π interaction) were described as following:

(i) The contribution of the interaction with minerals (Q_{im}) was calculated as the difference between adsorption amount of Zn^{2+} on CMBx and DCMBx.[23,24] In addition, (Fig. 1) the yield of

DCMBx from CMBx was considered to offset the concentration effect. The calculation formula is as following eqn (1):

$$Q_{im} = Q_o - Q_d \times Y \tag{1}$$

where Q_{im} (mg g^{-1}) is the adsorbed amount of Zn^{2+} ascribed to the interaction with minerals Q_o (mg g^{-1}); Q_d (mg g^{-1}) is the adsorption capacity of Zn^{2+} on CMBx or DCMBx, respectively; Y is the yield of DCMBx from CMBx.

(ii) The adsorption capacity Q_{ec} resulting from exchange with cation (K$^+$, Na$^+$, Ca^{2+}, and Mg^{2+}) was determined by calculating the net release of these cations before and after adsorption in solution (as shown by eqn (2)).

$$Q_{ec} = Q_K + Q_{Na} + Q_{Ca} + Q_{Mg} \tag{2}$$

where Q_K, Q_{Na}, Q_{Ca} and Q_{Mg} are the net released amounts of K$^+$, Na$^+$, Ca^{2+}, and Mg^{2+} from CMBx to solution after Zn^{2+} adsorption, respectively (mg g^{-1}).

(iii) The effects of interaction with minerals on Zn^{2+} adsorption includes precipitation with minerals and exchange with cations. Therefore, the adsorption capacity of Zn^{2+} due to precipitation with minerals could be calculated according to the difference between the Q_{im} and the Q_{ec} values (as shown in eqn (3)).

$$Q_{pm} = Q_{im} - Q_{ec} \tag{3}$$

(iv) A decrease in pH before and after Zn^{2+} adsorption on DCMBx was due to the interaction of Zn^{2+} with the surface acid functional groups (as shown in eqn (4)). The amount of H$^+$ released could be calculated by the decreased pH value, and then the amount of Zn^{2+} adsorbed by the surface acid functional groups complexation (Q_{cfd}) could be calculated accordingly. The yield of DCMBx from CMBx (Y) was calculated to offset the concentration effect (as shown in eqn (5)).

$$–COOH/–OH + Zn^{2+} + H_2O \rightarrow –COOZn^+/–OZn^+ + H_3O^+ \tag{4}$$
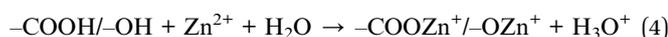
$$Q_{cf} = Q_{cfd} \times Y \tag{5}$$

(v) The adsorption capacity of other potential mechanisms (Q_{op}), including physical adsorption and Zn^{2+}–π interaction, could be calculated by subtracting the interaction with minerals (Q_{im}) and complexation with acid functional groups (Q_{cf}) from the total adsorption capacity (as shown in eqn (6)).

$$Q_{op} = Q_o - Q_{im} - Q_{cf} \tag{6}$$

In addition, the proportions of the contributions of different mechanisms to the Zn^{2+} adsorption were defined by following the ratios Q_{pm}/Q_o, Q_{ec}/Q_o, Q_{cf}/Q_o and Q_{op}/Q_o.

2.4 Statistical analysis

The batch experiments of Zn^{2+} adsorption were performed in triplicate. Since the characterization of microstructures and other properties was only measured once, no statistical analysis was carried. The means and standard deviations were calculated by Microsoft 2007 Excel software, and the adsorption kinetics and isotherms were fitted using Origin 8.5. Correlations were analyzed with the Pearson test at $P = 0.01$ or 0.05 by SPSS 18.0.

3. Results and discussion

3.1 Biochar characterization

The major physicochemical properties of CMBx are shown in Table 1. With increasing pyrolytic temperature from 450 to 650 °C, lower mass yield of CMBx was obtained and the BET surface area increased from 63.46 to 76.76 m^2 g^{-1}, mainly due to the slow decomposition of organic matter and accumulation of minerals in the process of biomass pyrolysis, such as bone, muscle, fat, and connective tissue in the carp meat and bone meal.[17,25] This was consistent with the SEM images observation showing more pores but less white impurities on the surface of CMB650 compared to CMB 450 and CMB550 (Fig. S1†). In addition, it can be seen from the SEM images (Fig. S1†) that the cracks on the surface of biochars gradually increase and expand with the increasing pyrolysis temperature, resulting in the increase of pore volume. CMBx were alkaline and higher pyrolysis temperature resulted in much higher pH values, which could be attributed to the decomposition of acidic functional groups of biochar at higher pyrolysis temperature and the presence of abundant hydroxyapatite (HAP) on biochars because of high ingredient of HAP in bone (60–70%).[16,17] There was a significant correlation between the zeta potential of biochar at the initial pH and the pyrolysis temperature ($r = -0.999$, $P = 0.008$ and less than 0.01), indicating that the amount of negative charges on the surface of the biochars increased as the pyrolysis temperature increases, and the effect of electrostatic attraction on the adsorption of metal cations increased. According to the results of zeta potential, CMB650 had the highest stability in aqueous solution. The change of C, H, N and O contents in CMBx resulted in a decrease in the H/C ratios, which showed a significant negative correlation with the pyrolysis temperature (Fig. S2†), suggesting that CMB650 had been highly carbonized. The thermogravimetric (TG) and derivative thermogravimetry (DTG) curves of CMBx are shown in Fig. S3.† As the temperature ranging from 200 to 500 °C and 500 to 700 °C, the mass loss of CMB450, CMB550, and CMB650 were about 3.29, 5.50, 6.17% and 15.32, 8.90, 5.12%, respectively. The evaporation of moisture and structural bound water from the biochars, and the burning of organic matters including fat and proteins occurred at the temperature ranging from 200 to 500 °C, and decomposition of calcite and degradation of organics with strong thermal stability occurred at the temperature ranging from 500 to 700 °C.[25,26] Relative to CMB450 and CMB550, CMB650 had a high thermal stability. In short, pyrolysis temperature had a significant influence on the physicochemical properties of CMBx, which might have a profound influence on their adsorption mechanisms for Zn^{2+}.

3.2 Adsorption properties

The kinetic model has been widely used to evaluate the adsorption process of heavy metals on biochars.[8,15,21] The

Table 1 Physicochemical properties of biochars derived from carp meat and bone meal at different pyrolysis temperature

| Sample | Yield (%) | pH | S_{BET}^{a} (m² g⁻¹) | Elemental content (%) | | | | Atomic ratio | | | PV^{a} (m³ g⁻¹) | AP^{a} (nm) | ZP^{a} (mV) |
				C	H	N	O	O/C	H/C	(O + N)/C			
CMB450	34.37 ± 0.46a[b]	9.44 ± 0.02c	63.46	42.05	3.36	6.88	11.87	0.21	0.96	0.35	0.07	4.72	−50.8 ± 0.89c
CMB550	25.92 ± 0.18b	9.63 ± 0.02b	63.62	31.12	2.09	4.91	12.30	0.30	0.81	0.43	0.14	8.90	−55.1 ± 0.70b
CMB650	19.48 ± 0.66c	9.87 ± 0.03a	76.76	30.81	1.21	5.16	13.58	0.33	0.43	0.47	0.16	8.52	−59.6 ± 0.75a

[a] S_{BET}, PV, AP, and ZP are the BET surface area, pore volume, average pore size and zeta potential, respectively. [b] The different lowercase letters (a, b, and c) behind the data on the same column indicate significant difference, which is analyzed by the Duncan's multiple range test using SPSS 18.0.

adsorption kinetics of Zn^{2+} on CMB450, CMB550 and CMB650 are presented in Fig. 1a, and the parameters fitted by the kinetic models are listed in Table 2. All the correlation coefficients R^2 obtained using the pseudo second order kinetic model were greater than 0.997, which were much larger than those using the pseudo first order kinetic model. In addition, the calculated adsorption capacities (Q_{cal}) based on the pseudo second order kinetic model were more accordant with the experimental value (Q_{exp}) than on the pseudo first order kinetic model, indicating that the adsorption processes of Zn^{2+} on CMB450, CMB550 and CMB650 conformed to the pseudo second order kinetic model, and the adsorption processes were dominated by chemisorption.[15,27] Elovich model reflects the heterogeneous diffusion process controlled by reaction rate and diffusion factor, which could be used to better evaluate the importance of chemical adsorption than the pseudo second order kinetic model.[17,20] In this study, the correlation coefficients (R^2) of Elovich model for CMB650 were greater than 0.99 and significantly greater than those for CMB450 (0.86) and CMB550 (0.97). This shows that the dominance of chemisorption in the process of Zn^{2+} adsorption on CMB6500 was obviously stronger than those on CMB450 and CMB550. In short, with the increase of pyrolysis temperature, the ability of CMBx to adsorb Zn^{2+} became stronger and the dominant role of chemisorption was more obvious in the adsorption process.

The adsorption of Zn^{2+} on CMB450, CMB550 and CMB650 reached equilibrium within 420 min. The adsorptive amounts increased rapidly during the initial 40 min, which accounted for 74.5–92.9% of total amount of adsorption, and showed only a small increment over the subsequent period until adsorption reached equilibrium. This was a typical three-stage adsorption process, including an initial rapid increase, a period of weakening growth and the final equilibrium stage. The intra-particle diffusion model is helpful to determine processes and mechanisms of adsorption and evaluate rate controlling stages.[15,27] The adsorption of Zn^{2+} on CMBx showed the three stages including the first fast stage by external diffusion, slower stage by intra-particle diffusion, and the third stage by adsorption equilibrium (Fig. 1b). k_{d1} values corresponding to the first fast stage were higher than k_{d2} values, and the line fitted at the second stage did not pass through the coordinate origin, implying that the intra-particle diffusion was the main rate-limiting step but not the only rate-limiting step mechanisms. Values of the intercept c_i (Table 2), which could reflect the thickness of the adsorbent boundary layer, were greater than 0 for all biochars, and the values of c_2 were higher than c_1. These findings indicate that the transport process of Zn^{2+} from solution to biochar particle through the boundary layer might influence the associated adsorption kinetics.[13,15]

The adsorption isotherms of Zn^{2+} on CMBx are shown in Fig. 2 and the parameters fitted by Langmuir, Freundlich and Temkin models are listed in Table 3. The Langmuir model fitted the isothermal adsorption data well with higher correlation coefficient R^2 (0.995–0.999) than Freundlich model (0.880–
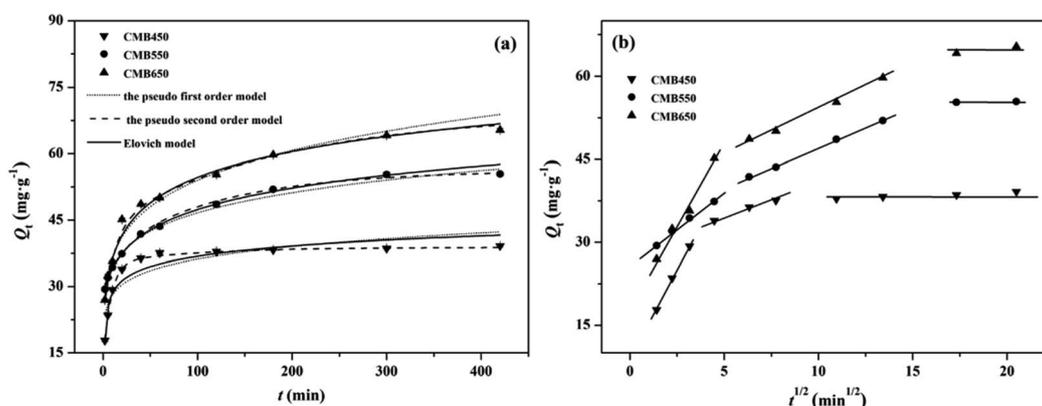

Fig. 1 Adsorption kinetics of Zn^{2+} on biochars and the fitting results of the pseudo first order model (a), the pseudo second order model (a), the Elovich model (a), and the intra-particle diffusion model (b).

Paper

Table 2 Kinetics parameters of Zn^{2+} adsorption on biochars using the pseudo first order, pseudo second order, Elovich and intra-particle diffusion models[a]

Sample	Q_{exp}	Pseudo first order model	Pseudo second order model	Elovich model	Intra-particle diffusion model	
CMB450	39.17	$Q_{cal} = 8.62$	$Q_{cal} = 39.22$	$\alpha = 19.05$	$k_{d1} = 6.56$	$k_{d2} = 1.14$
		$k_1 = 0.006$	$k_2 = 0.007$	$\beta = 3.82$	$c_1 = 8.64$	$c_2 = 28.93$
		$R^2 = 0.6708$	$R^2 = 0.9999$	$R^2 = 0.8668$	$R^2 = 0.9989$	$R^2 = 0.9853$
CMB550	55.44	$Q_{cal} = 22.54$	$Q_{cal} = 56.50$	$\alpha = 23.32$	$k_{d1} = 2.58$	$k_{d2} = 1.42$
		$k_1 = 0.007$	$k_2 = 0.002$	$\beta = 5.30$	$c_1 = 26.01$	$c_2 = 32.56$
		$R^2 = 0.9903$	$R^2 = 0.9982$	$R^2 = 0.9785$	$R^2 = 0.9939$	$R^2 = 0.9988$
CMB650	65.34	$Q_{cal} = 28.91$	$Q_{cal} = 66.23$	$\alpha = 20.90$	$k_{d1} = 5.78$	$k_{d2} = 1.59$
		$k_1 = 0.009$	$k_2 = 0.001$	$\beta = 7.40$	$c_1 = 18.79$	$c_2 = 38.20$
		$R^2 = 0.9609$	$R^2 = 0.9976$	$R^2 = 0.9911$	$R^2 = 0.9847$	$R^2 = 0.9939$

[a] Q_{exp} (mg g^{-1}) and Q_{cal} (mg g^{-1}) are the amount of Zn^{2+} adsorption at equilibrium and the adsorption capacity calculated by the pseudo first order and pseudo second order models at equilibrium, respectively. k_1 (min^{-1}), k_2 (g mg^{-1} min^{-1}) and k_{di} (mg g^{-1} min$^{-1/2}$) are the rate constant of the pseudo first order equation, the rate constant of the pseudo second order equation and the intra-particle diffusion equation, respectively. α (mg g^{-1} min^{-1}) and β (g mg^{-1}) are the initial adsorption rate constant and a parameter of the Elovich equation, respectively. c_i is representing the thickness of the liquid film, mg g^{-1}.
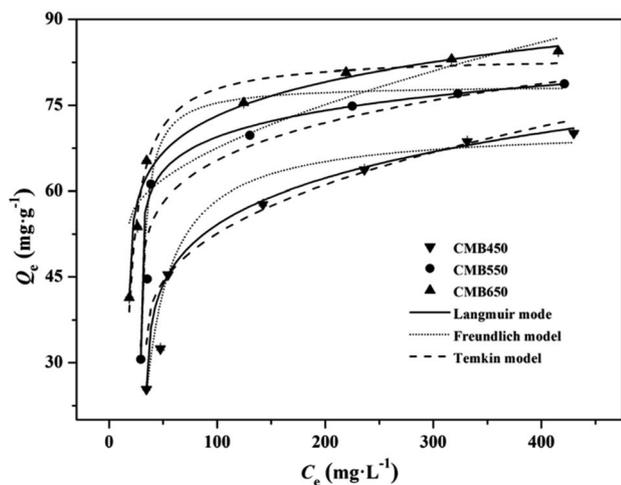
Fig. 2 Adsorption isotherms of Zn^{2+} on biochars with Langmuir model, Freundlich model and Temkin model fitting curves, respectively.

0.716), implying that the adsorption mechanisms of Zn^{2+} on CMBx were mainly dominated by chemical adsorption, and the monolayer adsorption occurred on the homogeneous surfaces

of CMBx.[20,21] In the fitting of Langmuir model, the R^2 value of CMB650 (0.9996) was obviously higher than those of CMB450 (0.9952) and CMB550 (0.9951), indicating that the predominant role of chemisorption of high temperature biochars was more significant for CMB650, which was consistent with the kinetic results. The parameter K_L was related to the affinity of the binding sites and represents the affinity between biochars and heavy metal ions. On the basis of K_L values, CMB650 had a higher affinity for Zn^{2+} than CMB450 and CMB550 (Table 3).[13] Additionally, the calculated maximum monolayer adsorption capacities based on Langmuir model for CMBx were 80.65–87.72 mg g^{-1}. The observed maximum monolayer adsorption capacities of CMBx for Zn^{2+} were higher than those of rice straw biochars (39.7 and 40.2 mg g^{-1}),[18,28] chicken manure biochars (11.2 mg g^{-1}),[18] sewage sludge biochars (4.3 mg g^{-1}),[18] wheat straw biochars (41.8 mg g^{-1}),[5] *S. hermaphrodita* biochars (48.1 mg g^{-1}),[5] hardwood biochars (4.3 mg g^{-1})[27] and corn straw biochars (4.3 mg g^{-1}),[27] suggesting that carp biochar was a promising one for Zn^{2+} adsorption (Table S1†). The R_L values (ESI†) for CMB450, CMB550 and CMB650 were obtained in the range of 0.091–0.455, 0.063–0.357 and 0.032–0.217, respectively, indicating that the adsorption of Zn^{2+} on CMBx was the favorable adsorption ($0 < R_L < 1$).[13,29] Moreover, the Temkin equation

Table 3 Isothermal adsorption parameters of Zn^{2+} adsorption on biochars obtained from the Langmuir, Freundlich, and Temkin isotherm model[a]

Sample	Langmuir model			Freundlich model			Temkin model		
	K_L	Q_m	R^2	K_F	n	R^2	K_T	A	R^2
CMB450	0.02	80.65	0.9952	8.32	0.37	0.8801	5.91	17.10	0.9427
CMB550	0.03	84.75	0.9951	17.22	0.27	0.7163	1.50	14.62	0.8056
CMB650	0.06	87.72	0.9996	27.92	0.19	0.8478	2.96	12.31	0.9061

[a] K_L (L mg^{-1}), K_F [mg$^{(1-1/n)}$ L$^{1/n}$ g^{-1}], and K_T (L mg^{-1}) are the adsorption coefficient of the Langmuir model, Freundlich model and Temkin model. Q_m is the maximum adsorption capacity calculated by Langmuir model, mg g^{-1}. The dimensionless constant n is experimentally derived exponent of Freundlich model. A (kJ mol^{-1}) is a coefficient related to the heat of adsorption in the Temkin model.

also fitted the adsorption data well, suggesting that Zn^{2+} adsorption process might be partly affected by the adsorbate/adsorbent interactions.[13]

3.3 Qualitative characterization of adsorption mechanisms

According to previous research results,[30–32] there are four main mechanisms for biochars to adsorb Zn^{2+}, including cation exchange between protons or alkaline metals and Zn^{2+}, complexation with functional groups, precipitation with minerals, and electrostatic interaction between biochar and Zn^{2+}.

Large amounts of metal cations (such as K^+, Na^+, Ca^{2+} and Mg^{2+}) were retained on the biochar by electrostatic attraction, forming complexes with functional groups (e.g., $-COO^-$, $-R-O^-$ and $C=C$) or precipitation.[15,17,22] These metals could be exchanged by Zn^{2+} during adsorption process. To confirm the above mechanism, the net release of metals ions was investigated, which was calculated from the difference between the release amount of metal ions from biochars in salt solution (0.01 M $NaNO_3$) (as the background electrolyte) and Zn^{2+} solution (100 mg L^{-1}) with 0.01 M $NaNO_3$ (Fig. 3). As shown in Fig. 3, significant amounts of K^+, Na^+, Ca^{2+} and Mg^{2+} were released into solution during the Zn^{2+} adsorption on CMB450, CMB550 and CMB650, and the total amounts of metal ions released were 0.44, 0.97 and 1.25 meq g^{-1}, respectively, where the release of divalent cations (Ca^{2+} and Mg^{2+}) was significantly higher than that of monovalent cations (K^+ and Na^+), and Ca^{2+} played a dominant role in these released cations because its release amount accounted for 79%, 83% and 81% of the total release, respectively. This was mainly due to two reasons. The first was that the monovalent cation could be retained on biochars by electrostatic attraction,[14,15] and could not be complexed with the functional groups or formed precipitates on the surface of the biochars, while the divalent cations could be retained on biochars by precipitation with CO_3^{2-} and PO_4^{3-} or complexation with functional groups (e.g., $-COOCa^+/Mg^+$, $-R-O-Ca^+/Mg^+$ and $Ca^+/Mg^+-\pi$).[13–15] Secondly, there were a lot of hydroxyapatite

(HAP, $Ca_4^I Ca_6^{II}(PO_4)_6(OH)_2$) in animal derived biochars,[16,17] and Ca^I and Ca^{II} were considered to be stable and exchangeable, respectively, indicating that the large number of exchangeable crystal lattice metal cations in HAP crystal structures could exchange with Zn^{2+}. The characterization results of XRD (Fig. S4†) and SEM-EDS (Fig. S5–S7†) could provide direct evidence. Both the distribution of Ca–P–O in CMBx surface and Ca–P–O–Zn in CMBx + Zn surface exhibited a notable correlation before and after Zn^{2+} adsorption in the elemental dot maps of EDS spectra, and such correlations increased as the pyrolysis temperature of biochar increased, which indicated that the pyrolysis temperature had a significant effect on the adsorption mechanism of Zn^{2+}.

The research by Xue et al. showed that precipitation occurred between Zn^{2+} and PO_4^{3-} released from animal (cattle) derived biochars.[20] Compared with the CMBx, a larger number of white granular crystals were dispersedly scattered on the surfaces of CMBx + Zn according to the results of SEM images (Fig. S1†). Analysis of the FTIR results of Zn^{2+} loaded biochars showed that, after Zn^{2+} adsorption, the peaks at 2013, 1029, 563 and 468 cm^{-1} (assigned to the v_1, v_3, v_4 and v_2 modes of PO_4^{3-}) had a significant displacement and stronger,[16,17,20] and the new peak at 603 cm^{-1} was attributed to the formation of Zn–O (Fig. S8†).[33] In addition, the stability of metal ions forming precipitates in solution was closely related to the solubility product constant (K_{sp}). For example, for Ca^{2+}, Mg^{2+} and Zn^{2+}, K_{sp} values of $Ca_3(PO_4)_2$ and $Mg_3(PO_4)_2$ are 2.07×10^{-29} and 1.04×10^{-24} respectively, which are significantly larger than K_{sp} values of precipitates $Zn_3(PO_4)_2$ (9.0×10^{-33}). That is to say, Zn^{2+} could form precipitates to be adsorbed on biochars through ion exchange with metal ions. XRD analysis proved that the precipitate formed on the surface of CMBx was zinc phosphate (Fig. S4†), which was similar to the results of Xue et al.[20]

Complexation of Zn^{2+} with functional groups through ion exchange has been suggested as an important mechanism for Zn^{2+} adsorption on biochars, including unsaturated carbon (e.g. $C=C$) and ionized oxygen-containing functional groups (e.g. hydroxyl and carboxyl groups).[18,20,34] Compared with the original biochar, the FTIR results of Zn^{2+} loaded biochars showed that, after Zn^{2+} adsorption, the peaks at 3498, 3034 and 1649 cm^{-1} (assigned to the –OH, –CO–OH and $C=C$) had a significant displacement and were broadened, indicating that the hydroxyl, carboxyl and $C=C$ were involved in the adsorption process of Zn^{2+} on CMBx. Analysis of the XPS wide scan spectra show that, after Zn^{2+} adsorption on CMB550, the photoelectron peaks of Zn $2p_{1/2}$ and Zn $2p_{3/2}$ appeared in the binding energy of 1022.13 eV and 1045.31 eV (Fig. 4f), respectively, indicating that Zn^{2+} were adsorbed on CMB550 successfully;[7,18] the binding energy of $C=C$/OFGs in C 1s/O 1s XPS spectra had a minor shift due to the interaction between Zn^{2+} and π electrons/OFGs.[18] In order to further explain the mechanism of functional groups in the adsorption reaction, simpler biochar molecules containing $C=C$, hydroxyl and carboxyl groups (e.g., benzene rings, catechol or phthalic acid) were used to model the interactions between biochar and Zn^{2+}. The binding energy between the heavy metal ions (Ca^{2+}, Mg^{2+} or Zn^{2+}) and the benzene, catechol or phthalic acid were calculated using the G09 package. M^{2+}–

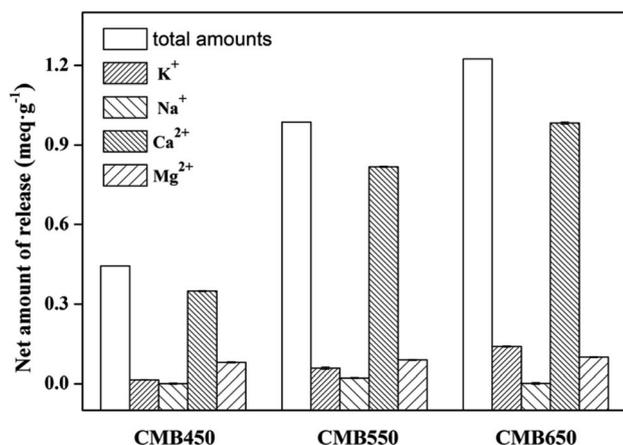**Fig. 3** The net amount of released cations (K^+, Na^+, Ca^{2+} and Mg^{2+}) from the mixed solution of CMBx with and without Zn^{2+} after equilibration.
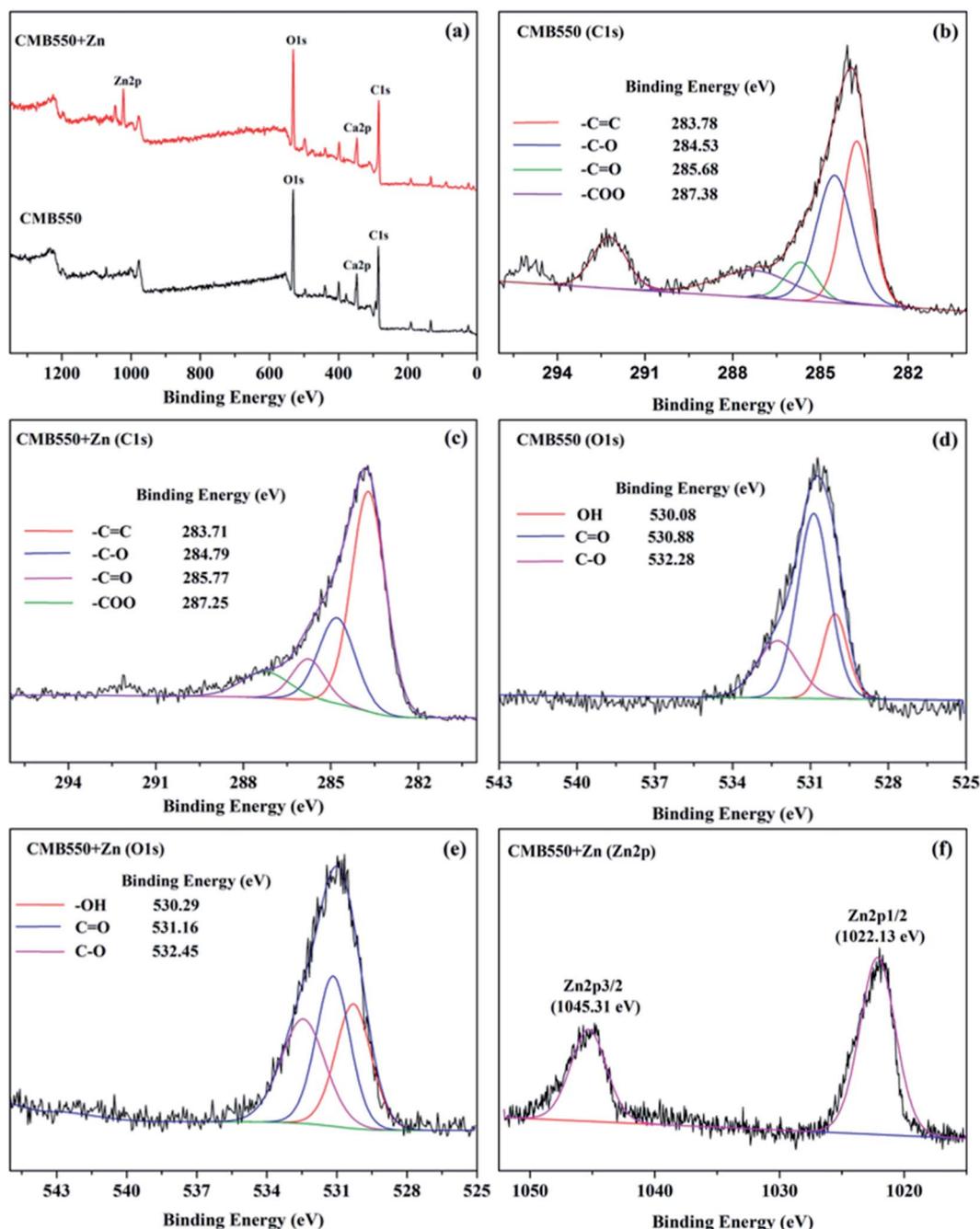
Fig. 4 XPS spectra of CMB550 and CMB550 + Zn (a), high resolution spectra of C 1s (b and c), O 1s (d and e) and Zn 2p (f).

C_6H_6, $M^+–C_6H_5O_2$ or $M^+–C_6H_5O_4$ complexes were calculated at the B3LYP/6-311+G** level (M = Ca, Mg or Zn). The binding energy between the heavy metal ions (Ca^{2+}, Mg^{2+} and Zn^{2+}) and the benzene, catechol or phthalic was calculated (ESI†), and the results of the optimized stable structure of the $M^{2+}–C_6H_6$, $M^+–C_6H_5O_2$ or $M^+–C_6H_5O_4$ complexes and its corresponding binding energy are shown in Fig. 5. For benzene ring, the binding energy for Ca^{2+} (83.9 kcal mol^{-1}) and Mg^{2+} (118.1 kcal mol^{-1}) with benzene ring *via* the combination mode of surface complexation was smaller than that for Zn^{2+} (160.5 kcal mol^{-1}); therefore, it was easier for Zn^{2+} complexes

with benzene ring through ion exchange with Ca^{2+} and Mg^{2+}. Similar results were obtained when catechol or phthalic acid combined with Ca^{2+}, Mg^{2+} and Zn^{2+}. The binding energy difference between benzene ring and Zn^{2+} (160.5 kcal mol^{-1}) was smaller compared to that of catechol (430.5 kcal mol^{-1}) and phthalic acid (424.5 kcal mol^{-1}), suggesting that Zn^{2+} adsorption occurred more easily on carboxyl and hydroxyl groups than on C=C. $Zn^{2+}–\pi$ interaction had a certain contribution to Zn^{2+} adsorption on CMBx but its effect was far less than that of OFGs. There was a fascinating phenomenon: for phthalic acid, since the radius of Zn^{2+} ion was smaller than that of Ca^{2+} or
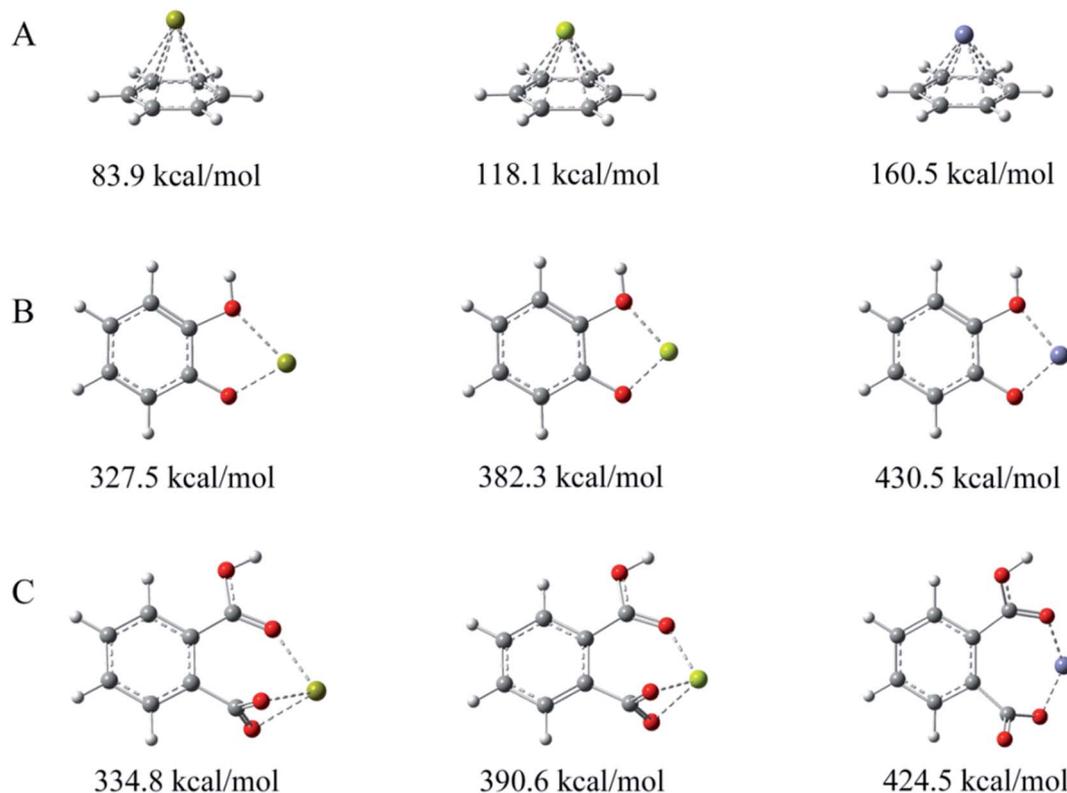
Fig. 5 Calculated the most stable conformations of the binding energy between benzene ring (A), catechol (B) and phthalic acid (C) with Mg^{2+}, Ca^{2+}, and Zn^{2+}. Spheres with gray, white, red, greyish green, green and purple colors represent C, H, O, Mg^{2+}, Ca^{2+}, and Zn^{2+}, respectively.

Mg^{2+}, the stable structure formed by complexing Zn^{2+} with phthalic acid was a quasi-planar seven-membered ring, while the larger radius of Ca^{2+} and Mg^{2+} were not conducive to the formation of seven-membered ring and eventually coordinated with the three oxygen to form a stable structure.

The occurrence of complexation of Zn^{2+} with OFGs (e.g., –COOH, –OH) was usually accompanied by the release of H^+ into solution, causing the pH value of solution to decrease.[13,21,35] Demineralized biochars (DCMBx) were used to explore the release of H^+ due to the occurrence of complexation of Zn^{2+} with –OH or –COOH in the Zn^{2+} adsorption process. The results showed that there was a decreasing trend of pH value after Zn^{2+} adsorption and the decrease of pH values was more significant for DCMB450 than for DCMB650 (Fig. S9†), indicating that the occurrence of complexation of Zn^{2+} with OFGs might contribute more for the low temperature biochars than high temperature biochars. In summary, the pyrolysis temperature had a significant effect on the adsorption mechanism.

3.4 Quantitative characterisation of adsorption mechanisms

According to the adsorption of Zn^{2+} on the original biochars or demineralized biochars and related control experiments, the contribution of different mechanisms to the Zn^{2+} adsorption were calculated. The contributions of precipitation with minerals (Q_{pm}), exchange with cation (Q_{ec}), complexation with OFGs (Q_{cf}) and other potential mechanisms (Q_{op}) to the total Zn^{2+} adsorption (Q_o) are shown in Fig. 6. As the pyrolysis temperature increased from 450 to 650 °C, the contribution of both Q_{ec} and Q_{ec}/Q_o increased, while those of Q_{cf} and Q_{cf}/Q_o showed the reverse trend. Specifically, the values of Q_{ec} and Q_{ec}/Q_o for CMB450 were 12.4 mg (Zn) g^{-1} and 31.5%, respectively, while those for CMB650 were 40.7 mg (Zn) g^{-1} and 61.2% respectively (Fig. 6). On the contrary, the values of Q_{cf} and Q_{cf}/Q_o for CMB450 were 16.3 mg (Zn) g^{-1} and 41.7%, respectively, while those for CMB650 were 3.15 mg (Zn) g^{-1} and 4.7% respectively. This phenomenon indicated that the contribution of complexation with OFGs to adsorption in high-temperature biochar was reduced, which was supported by the correlation between the pyrolysis temperature and the carbonization degree of biochars (Fig. S2†). In addition, the BET specific surface area and pore volume of biochars increased as the pyrolysis temperature increased (Table 1), which would cause more ion exchange between Ca^{2+} (from HAP crystal structures) and Zn^{2+}. More HAP crystal structures would be exposed with the higher temperature carbonization of fish bones. Therefore, the exchange with cation dominated the process of adsorption of Zn^{2+} by high-temperature biochars, while the complexation with OFGs dominated the process by low-temperature biochar. The values of Q_{pm} and Q_{pm}/Q_o for CMB650 were higher than those for CMB450 and CMB550, indicating that the precipitation mechanism was more obvious for CMB650, because CMB650 had the highest pH value. However, the values of Q_{op} and Q_{op}/Q_o for CMB450 were lower than those for CMB550 and CMB650, indicating that the other potential mechanisms, including physical adsorption, Zn^{2+}–π interaction and electrostatic attraction, were not obvious for CMB450 compared to
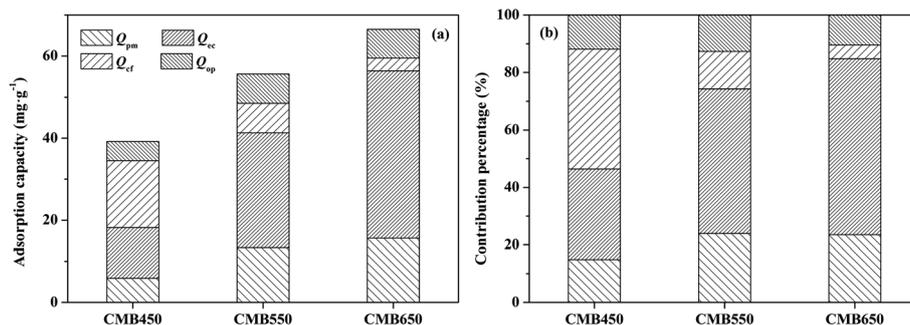
Fig. 6   (a) The contribution percentage of different mechanisms to Zn^{2+} adsorption on CMBx, (b) relative contribution of each mechanism to total adsorption (Q_o), including precipitation with minerals (Q_{pm}), exchange with cation (Q_{ec}), complexation with OFGs (Q_{cf}), and other potential mechanisms (Q_{op}).

CMB550 and CMB650, because CMB450 had the lowest BET surface area, aromaticity and zeta potential (Table 1).

Overall, the pyrolysis temperature had an important influence on the adsorption performance of Zn^{2+} on CMBx and the contribution of different mechanisms. With the pyrolysis temperature increased, the effect of the minerals on Zn^{2+} adsorption ($Q_{ec}/Q_o + Q_{pm}/Q_o$) increased significantly, while the contribution of OFGs decreased. The value of Q_{im} ($Q_{ec} + Q_{pm}$) for CMBx accounted for 46.4–84.8% of their total adsorption, indicating that the mechanisms of Zn^{2+} adsorption on CMB650 (84.8%) were dominated by the interaction between Zn^{2+} and the minerals. On the contrary, the mechanisms of Zn^{2+} on CMB450 was dominated by complexation with OFGs and exchange with cation due to the value of $Q_{cf}/Q_o + Q_{ec}/Q_o$ for CMB450 accounted for 73.2%. Considering the total adsorption capacity, 650 °C was the optimized pyrolysis temperature for the preparation of biochar from dead carp for treating Zn-contaminated wastewater.

4.   Conclusions

The adsorption of Zn^{2+} on CMBx was dependent on the effect of pyrolysis temperature on properties of biochar. CMB650 had a larger adsorption capacity for Zn^{2+} than other biochars. The kinetic and isothermal adsorption data could be best fitted by the pseudo second order model and the Langmuir model, respectively. The adsorption mechanism of Zn^{2+} on biochar mainly included precipitation with minerals, metal ion exchange and complexation with functional groups (e.g. hydroxy, carboxyl and C=C). The interaction with minerals including precipitation with the minerals and metal ion exchange dominated the Zn^{2+} adsorption on CMB550 and CMB650, while the contribution of complexation with OFGs and metal ion exchange were the dominant mechanism in combining Zn^{2+} with CMB450. Therefore, CMB650 has great potential as an engineering adsorbent to treat Zn-contaminated wastewater.

Conflicts of interest

There are no conflicts to declare.

Acknowledgements

References

1 E. Gozzard, W. M. Mayes, H. A. B. Potter and A. P. Jarvis, Environ. Pollut., 2011, 159, 3113–3122.

2 M. Mekapogu, J. Nadimikeri, P. K. Madri and S. Devi, Int. J. Sediment Res., 2018, 33, 510–517.

3 M. Chen, D. Wang, S. Ding, X. Fan, Z. Jin, Y. Wu, Y. Wang and C. Zhang, Sci. Total Environ., 2019, 670, 361–368.

4 J. Deng, D. Fu, W. Hu, X. Lu and H. Bryan, Bioresour. Technol., 2020, 303, 122963, DOI: 10.1016/ j.biortech.2020.122963.

5 A. Bogusz, P. Oleszczuk and R. Dobrowolski, Bioresour. Technol., 2015, 196, 540–549.

6 S. M. Sorouraddin and S. Nouri, Anal. Methods, 2016, 8(6), 1396–1404.

7 J. Song, S. Zhang, G. Li, Q. Du and F. Yang, J. Hazard. Mater., 2020, 391, 121692, DOI: 10.1016/j.jhazmat.2019.121692.

8 L. Gao, J. Deng, G. Huang, K. Li, K. Cai, Y. Liu and F. Huang, Bioresour. Technol., 2019, 272, 114–122.

9 F. M. Pellera, A. Giannis, D. Kalderis, K. Anastasiadou, R. Stegmann, J. Y. Wang and E. Gidarakos, J. Environ. Manage., 2012, 96, 35–42.

10 W. Yan and R. Liu, Sci. Total Environ., 2018, 628, 1139–1148.

11 H. Zheng, H. Mu and X. Zhao, Mar. Policy, 2018, 96, 152–162.

12 W. Qiao, Y. Zhang, X. Xu and L. Zhu, Ind. Water Treat., 2019, 39(10), 26–31.

13 X. Cui, S. Fang, Y. Yao, T. Li, Q. Ni, X. Yang and Z. He, Sci. Total Environ., 2016, 562, 517–525.

14 Z. Mahdi, Q. J. Yu and A. E. Hanandeh, J. Environ. Chem. Eng., 2018, 6, 1171–1181.

15 Y. Deng, S. Huang, D. A. Larid, X. Wang and Z. Meng, Chemosphere, 2019, 218, 308–318.

16 S. Lei, Y. Shi, Y. Qiu, L. Che and C. Xue, Sci. Total Environ., 2019, 646, 1281–1289.

17 S. Lei, L. Zhu, C. Xue, C. Hong, J. Wang, L. Che, Y. Hu and Y. Qiu, *Environ. Pollut.*, 2019, **258**, 113675, DOI: 10.1016/j.envpol.2019.113675.

18 M. Zhao, Y. Dai, M. Zhang, C. Feng and R. Qiu, *Sci. Total Environ.*, 2020, **717**, 136894, DOI: 10.1016/j.scitotenv.2020.136894.

19 A. R. Betts, N. Chen, J. G. Hamilton and D. Peak, *Environ. Sci. Technol.*, 2013, **47**, 14350–14357.

20 C. Xue, L. Zhu, S. Lei, M. Liu and Y. Qiu, *Sci. Total Environ.*, 2020, **713**, 136395, DOI: 10.1016/j.scitotenv.2019.136395.

21 Z. Wang, G. Liu, H. Zheng, F. Li, H. H. Ngo, W. Guo, C. Liu, L. Chen and B. Xing, *Bioresour. Technol.*, 2015, **177**, 308–317.

22 R. Wang, D. Huang, Y. Liu, C. Zhang, C. Lai, G. Zeng, M. Cheng, X. Gong, J. Wan and H. Luo, *Bioresour. Technol.*, 2018, **261**, 265–271.

23 Y. Qiu, H. Cheng, C. Xu and G. D. Sheng, *Water Res.*, 2008, **42**, 567–574.

24 D. I. Mendoza-Castillo, A. Bonilla-Petriciolet and J. Jáuregui-Rincón, *Water Treat.*, 2015, **54**, 1651–1662.

25 X. Cao and W. Harris, *Bioresour. Technol.*, 2010, **101**, 5222–5228.

26 Y. Xu and B. Chen, *Bioresour. Technol.*, 2013, **146**, 485–493.

27 X. Chen, G. Chen, L. Chen, Y. Chen, J. Lehmann, M. B. McBride and A. G. Hay, *Bioresour. Technol.*, 2011, **102**, 8877–8884.

28 J. H. Park, J. J. Wang, S. H. Kim, J. S. Cho, S. W. Kang, R. D. Delaune, K. J. Han and D. C. Seo, *Colloids Surf., A*, 2017, **533**, 330–337.

29 L. Wang, Y. M. Xu, X. F. Liang, Y. B. Sun and R. Y. Dong, *China Environ. Sci.*, 2014, **11**, 2851–2858.

30 H. Lu, W. Zhang, Y. Yang, X. Huang, S. Wang and R. Qiu, *Water Res.*, 2012, **46**, 854–862.

31 M. I. Inyang, B. Gao, Y. Yao, Y. Xue, A. Zimmerman, A. Mosa, P. Pullammanappallil, Y. S. Ok and X. Cao, *Crit. Rev. Environ. Sci. Technol.*, 2016, **46**, 406–433.

32 H. Li, X. Dong, E. B. D. Silva, L. M. de Oliveira, Y. Chen and L. Q. Ma, *Chemosphere*, 2017, **178**, 466–478.

33 R. Fernández-González, M. A. Martín-Lara, J. A. Moreno, G. Blazquez and M. Calero, *J. Cleaner Prod.*, 2019, **227**, 634–663.

34 Z. L. Chen, J. Q. Zhang, L. Huang, Z. H. Yuan, Z. J. Li and M. C. Liu, *J. Integr. Agric.*, 2019, **18**(1), 201–210.

35 X. Cao, L. Ma, B. Gao and W. Harris, *Environ. Sci. Technol.*, 2009, **43**, 3285–3291.